System and Control Design of a Voice Coil Actuated Mechanically Decoupling Two-body Vibration Isolation System

Ernst Csencsics, Markus Thier, Reinhard Hainisch, and Georg Schitter, *Senior Member, IEEE*

***Abstract*—Structural modes such as decoupling of a mechanical subsystem are in general unwanted effects in high precision positioning systems. This paper introduces intentional decoupling as a design choice by using a connecting flexure-damper configuration that allows high bandwidth control of a stiff first subsystem and lower bandwidth control of a bulky second subsystem at the same time. An experimental setup of a single DoF system with one body intentionally decoupling above 190 Hz is developed and analyzed, showing good agreement with the analytical modeling. A model-based H_∞-controller to actively control the position of the first body is designed and the damping in the system is revealed as an important design parameter to reduce the control effort around the decoupling frequency. It is demonstrated that with the derived controller the first and the second body of the resulting prototype can simultaneously be controlled with bandwidths of 1.4 kHz and 180 Hz, respectively. When exposed to a disturbance profile with 12.4 μm rms value in the laboratory environment the remaining rms positioning errors for the actively and passively controlled subsystems are as small as 0.12 μm and 0.81 μm, respectively.**

***Index Terms*—Vibrations, Optimal control, System analysis and design**

I. Introduction

HIGH precision production, positioning and metrology systems require a high control bandwidth ensuring good disturbance rejection, in order to achieve the required levels of precision [1]. Since high precision tasks are in general sensitive to disturbances, external vibrations are a common problem [2]. Widely used countermeasures in these fields are passive [3], [4] and active vibration isolation systems [5], [6], equipped with sensors and actuators to actively reject external vibrations. Active concepts that employ closed loop control to maintain constant distance between a probe and a sample are also reported [7], [8]. Voice coil actuators are frequently used in such systems as they provide large stroke and have no mechanical connection between stator and mover [9]. This results in low stiffness systems that attenuate external vibrations significantly [7]. The control bandwidth of these systems typically lies above the suspension mode (1st resonance) of the system.

For such closed loop controlled active vibration isolation systems structural modes represent a challenge, as they in general may limit the achievable closed loop bandwidth of the system. At higher frequencies every lumped mass that is considered rigid at slow speeds shows internal structural modes, meaning additional system dynamics [1]. They arise either from structural modes of the individual components of the positioned structure, or their interconnections, as in the case of a decoupling sub-mass [10]. To cope with such unwanted effects strategies like active damping [11] are reported, which, however, requires an extended control structure. Another way to remove unwanted dynamics is overactuation [12], such as active suppression of vibrational modes with piezo actuators [13]. There are also control approaches for MIMO systems employing block decoupling algorithms to decouple vibrating structures into independent substructures [14]. The related drawback in these cases is clearly an increased system complexity. Further reported in literature is the placement of actuators in nodes of the respective unwanted mode [15] to avoid its excitation, which requires a rather complex preliminary system analysis and has disadvantages in the case of a broadband external excitation.

In contrast to active vibration isolation structural decoupling mechanisms are deliberately introduced in structures for passive vibration suppression, that in some cases outbalance active solutions with respect to costs, complexity and reliability [16]. To decrease the system transmissibility a stack of decoupling mechanisms with alternating layers of stiff masses and compliant springs with inherent viscoelastic damping is proposed [17]. With slightly displaced resonance frequencies the transmissibility of all layers is summed up to the entire system transmissibility. A similar approach with a two stage stacked decoupling mechanism is also reported [18]. Both systems have the drawback, that due to the additional stacked masses they become very heavy and thus require extremely high spring stiffness. In addition, mechanically decoupling sub-masses are used to decouple structural modes in a four degree of freedom micro-machined gyroscope to simplify design requirements and minimize instability and drift [19]. Recently also structures incorporating nonlinear stiffness and damping have been proposed for passive vibration isolation and the transmissibility of such systems has been investigated [20]. Besides a nonlinear spring mechanism incorporating a bistable composite plate [21] and an Euler buckled beam used as negative stiffness corrector [22] also a scissor-like structure with quasi-zero stiffness, beneficial nonlinear damping and adjustable vibration isolation performance is reported [23]. Such nonlinear structures are however rather complex in manufacturing, tuning and implementation.

The concept proposed in this paper uses an intended, well

The authors are with the Automation and Control Institute, Vienna University of Technology, A-1040 Vienna, Austria e-mail: csencsics@acin.tuwien.ac.at.

Post-print version of the article: E. Csencsics and M. Thier and R. Hainisch and G. Schitter, "System and control design of a voice coil actuated mechanically decoupling two-body vibration isolation system," *IEEE Transactions on Mechatronics*, vol. 23, no. 1, pp. 321-330, 2018. DOI: 10.1109/TMECH.2017.2771440

designed structural decoupling mode, known from passive systems, to improve the performance and versatility of an active vibration isolation system for a combined high precision metrology system. The system configuration considered is a metrology platform for inline metrology (see [7]) that comprises one position sensor, one compact high-precision metrology subsystem (*MS1*) and one bulky low-precision metrology subsystem (*MS2*), as shown in Fig. 1. A classical rigid design for this system configuration includes several performance limiting factors such as (i) the entire platform needs to fulfill the high precision requirements, (ii) a large moved mass (current limitations), and (iii) structural modes of *MS2*, at frequencies below the target bandwidth of *MS1*, are impairing the performance of *MS1*. The separation into two mechanically loosely coupled subsystems, as alternative to a rigid system design, allows the spectral separation of the two subsystems, meaning that different target bandwidths fulfilling the individual precision requirements are enabled. This approach has further the potential to avoid the excitation of performance limiting structural modes of *MS2* that lie above the target bandwidth of *MS2* (i.e. the decoupling resonance frequency) and below the target bandwidth of *MS1*.

This paper provides an analytic description of a single axis vibration isolation system with an intentionally decoupling subsystem and its design parameters, and shows that different control bandwidths can be achieved simultaneously for each subsystem using a single actuator together with a suitable controller design. In the system analysis in Section II the damping in the system is identified as an important design parameter to shape the system mechanics, in order to provide good robustness against variations of the decoupling dynamics and to maintain good transient performance of the decoupling subsystem. The single axis prototype is developed in Section III and analyzed in Section IV, matching the requirements derived in the analytic section. Based on identification data a controller is designed via H_∞-synthesis in Section V. Section VI evaluates the controlled system in terms of closed loop bandwidth, robustness against plant variations, disturbance rejection, resulting positioning error and change of operating point. Experiments demonstrate that for the proposed system the designed SISO feedback controller can be used to position the two bodies of the system with a high and a low bandwidth, respectively, at the same time.

II. System Modeling for Single Axis Decoupling System

Fig. 1 shows a high precision metrology system, that needs to be positioned in constant distance to a measurement sample while compensating external vibrations[1]. It comprises two sub-metrology-systems with (i) subsystem *MS1* (e.g. an atomic force microscope) being compact and mechanically stiff, requiring high precision and bandwidth, and (ii) subsystem *MS2* (e.g. a white light interferometer) being bulky, with structural modes around 300 to 400 Hz, requiring only low precision and bandwidth. The subsystems are connected via a

[1]Project "Automated in-line metrology for nanoscale production": www.aim4np.eu

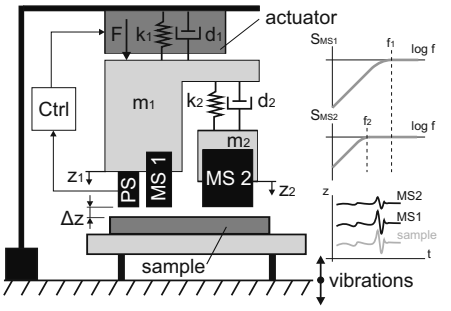

Fig. 1. Concept of positioning a high precision metrology system in constant distance to a sample. The system comprises a compact subsystem *MS1* (rigid body with m_1) and a bulky subsystem *MS2* (rigid body with m_2), requiring high and lower precision, respectively. The subsystems are connected via a designed spring-damper structure (k_2 and d_2). *MS1* is via k_1 and d_1 connected to mechanical ground and actuated by the force F. Its position is measured by a sensor (PS) and actively controlled (Ctrl). z_1 and z_2 are the vertical positions of the first and second body. *MS2* has good disturbance rejection up to f_2 and decouples from *MS1* above this frequency, leaving only *MS1* for improved disturbance rejection up to f_1.

flexure-damper structure. The high precision metrology system *MS1* is directly connected to the actuator and a positioning sensor measures its distance to the sample, which is disturbed by external vibrations. The flexure-damper structure can be designed such that the bulky subsystem *MS2* decouples from subsystem *MS1* above a defined decoupling frequency. Decoupling thereby means that MS2 can no longer follow the motion of MS1, leaving only the small body for high bandwidth vibration cancellation.

To model the dynamic behavior of a mechanical system that is decoupling along a single degree of freedom a two-body mechanical lumped mass model (see Fig.1) is considered. The first rigid body with mass m_1 is connected to mechanical ground via a spring k_1 and a damper d_1. The second rigid body with mass m_2 is connected to the first body via a second spring k_2 and a second damper d_2. The system is actuated via a force F on the first body by an actuator that is installed in parallel to the spring k_1. The coordinates z_1 and z_2 represent the vertical positions of the first and second body, respectively. The differential equations describing the motion for the two bodies are:

$$\begin{aligned} m_1\ddot{z_1}(t) = F &- k_1 z_1(t) - k_2(z_1(t) - z_2(t)) \\ &- d_1\dot{z_1}(t) - d_2\left(\dot{z_1}(t) - \dot{z_2}(t)\right), \end{aligned} \tag{1}$$

and

$$m_2\ddot{z_2}(t) = k_2(z_1(t) - z_2(t)) + d_2\left(\dot{z_1}(t) - \dot{z_2}(t)\right). \tag{2}$$

The transfer functions (TFs) from the applied force F to the vertical positions z_1 and z_2 can be obtained by combining (1) and (2), and by applying the Laplace transformation for null starting conditions ($z_1(0)$=$z_2(0)$=0). This results in

$$\frac{Z_1(s)}{F(s)} = \frac{m_2 s^2 + d_2 s + k_2}{m_1 m_2 s^4 + D_3 s^3 + D_2 s^2 + D_1 s + k_1 k_2} \tag{3}$$

for the position of the first body, and in

$$\frac{Z_2(s)}{F(s)} = \frac{d_2 s + k_2}{m_1 m_2 s^4 + D_3 s^3 + D_2 s^2 + D_1 s + k_1 k_2}, \tag{4}$$

Post-print version of the article: E. Csencsics and M. Thier and R. Hainisch and G. Schitter, "System and control design of a voice coil actuated mechanically decoupling two-body vibration isolation system," *IEEE Transactions on Mechatronics*, vol. 23, no. 1, pp. 321-330, 2018. DOI: 10.1109/TMECH.2017.2771440

for the position of the second body, with

$$D_1 = d_1k_2 + d_2k_1, \tag{5}$$
$$D_2 = d_1d_2 + k_1m_2 + k_2m_1 + k_2m_2, \tag{6}$$
$$D_3 = d_1m_2 + d_2m_1 + d_2m_2. \tag{7}$$

The relation between the position of the first and the second body is obtained by dividing (4) by (3) resulting in

$$G_{z2,z1}(s) = \frac{Z_2(s)}{Z_1(s)} = \frac{d_2s + k_2}{m_2s^2 + d_2s + k_2}. \tag{8}$$

As damping does in general not dominate the dynamics of mechatronic positioning systems [24], it is neglected for the frequency approximations of poles and zeros made in the following. The TF of the first body has an anti-resonance (pair of conjugate complex zeros) at

$$f_a = \frac{1}{2\pi} \cdot \sqrt{k_2/m_2}, \tag{9}$$

while the TF of the second body has a zero at

$$f_z = \frac{1}{2\pi} \cdot k_2/d_2. \tag{10}$$

The poles are the same for both TFs and with the mass and spring ratio $g_m = m_1/m_2$ and $g_k = k_1/k_2$ their frequencies can be modeled by

$$f_1 = \frac{1}{2\pi} \cdot \sqrt{k_1/(m_1 + m_2)}, \tag{11}$$

and

$$f_2 = f_a \cdot \sqrt{(g_k + g_m + 1)/g_m}. \tag{12}$$

The shapes of the TFs of the first and the second body of a theoretical system model with different values of d_2 can be obtained from the simulated plots in Fig. 2(a) and Fig. 2(b), respectively. The parameters for the depicted model are listed in Table I, where m_1 and m_2 correspond to the masses of the experimental setup. The resulting system dynamics can in general vary significantly depending on the different parameter combinations of masses, springs and dampers [25]. For the considered case of a low stiffness actuated system with a small inner, a large outer mass and a desired decoupling mode above the suspension mode, the dynamics will, however, always look as shown in Fig. 2.

TABLE I
PARAMETERS OF THEORETICAL TWO-BODY SYSTEM MODEL.

Parameter	Value	Unit
m_1	1.4	kg
m_2	4.3	kg
k_1	23e3	N/m
k_2	17e5	N/m
d_1	10	N·s/m

The TFs of the first and the second body show a resonance (suspension mode) around f_1=10 Hz, followed by a -40 dB line, which is the mass line of the total mass m_1+m_2 (rigidly moving single body system), with a related -180° phase. At around f_a=100 Hz the first body shows an anti-resonance, which lifts the phase. In the undamped case (d_2=0, ideal case) the movement of the second body at this frequency is such, that the corresponding strain of the spring creates a force that exactly compensates the external force acting on the first body. Meaning that the first body stops moving at f_a and all force is directly transferred to the second body. At f_2=203 Hz both bodies show the decoupling resonance. Thereafter the TF of the first body continues with a -40 dB mass line (phase at -180°) determined by its own mass only. The TF of the second body continues in the undamped case with a -80 dB slope and a phase at -360°, meaning that the two bodies are moving in counter phase above the decoupling resonance. This inability of the second body to follow the movement of the first body at frequencies above the decoupling resonance is called *decoupling of the second body* [1].

The mass line of the first body above f_2 is vertically lifted to a higher level compared to the mass line before the decoupling, as only the mass m_1 of the first body remains when the second mass has decoupled. The vertical shift depends on the ratio of $m_1 + m_2$ to m_1 and is 12 dB for the chosen model parameters. This effect represents a design parameter that has the potential to reduce the energy consumption of the entire vibration isolation system.

It can be seen that a higher damping value d_2 reduces the peak heights of the anti-resonance and the decoupling resonance of both bodies. This design parameter is important for the controller design and will be revisited in Section V. Assuming a fixed spring constant k_2 the damping d_2 also determines the location of the zero f_z of the second body's TF (see. (10)). With increasing values of d_2 the zero is shifted to lower frequencies (e.g. d_2=100 $\rightarrow$ f_z=2.706 kHz), resulting in a 3rd order system behavior with a -60 dB slope (phase approaching -270°) above f_z. Compared to the -80 dB slope for low damping values (e.g. d_2=10 $\rightarrow$ f_z=27.06 kHz), this means that for high damping values, as f_z approaches f_2 e.g. d_2=800 $\rightarrow$ f_z=338.2 Hz), the decoupling between both bodies is decreased.

III. SINGLE AXIS DECOUPLING EXPERIMENTAL SETUP

To demonstrate the principle of mechanical decoupling a single axis experimental setup is used. Fig.3 depicts a schematic of the setup. It consists of a voice coil actuator (Shaker S51110, TIRA GmbH, Germany) that is placed on mechanical ground and is used for vertical actuation of the entire mechanical frame on top. The actuator is driven by a custom made current amplifier (Amplifier type MP38CL, Apex Microtechnology, Tucson, AZ, USA). The amplifier is controlled by a current controller with a bandwidth of 10 kHz, implemented on the FPGA of a dSpace-platform (Type: DS1005, dSPACE GmbH, Germany). The controller implementation is done on the processor of the dSpace-platform running at a sampling frequency of 20 kHz.

Referring to Fig. 1 the k_1 and d_1 correspond to the stiffness and damping inside the actuator, connecting the actuator mover A_M to the stator part A_S. The mechanical structure on top comprises an inner aluminium block (1.4 kg, connected to the actuator) and an outer aluminium frame (4.3 kg), which are connected via two leaf springs (brass, 2 mm thick, 300 mm

Post-print version of the article: E. Csencsics and M. Thier and R. Hainisch and G. Schitter, "System and control design of a voice coil actuated mechanically decoupling two-body vibration isolation system," *IEEE Transactions on Mechatronics*, vol. 23, no. 1, pp. 321-330, 2018. DOI: 10.1109/TMECH.2017.2771440

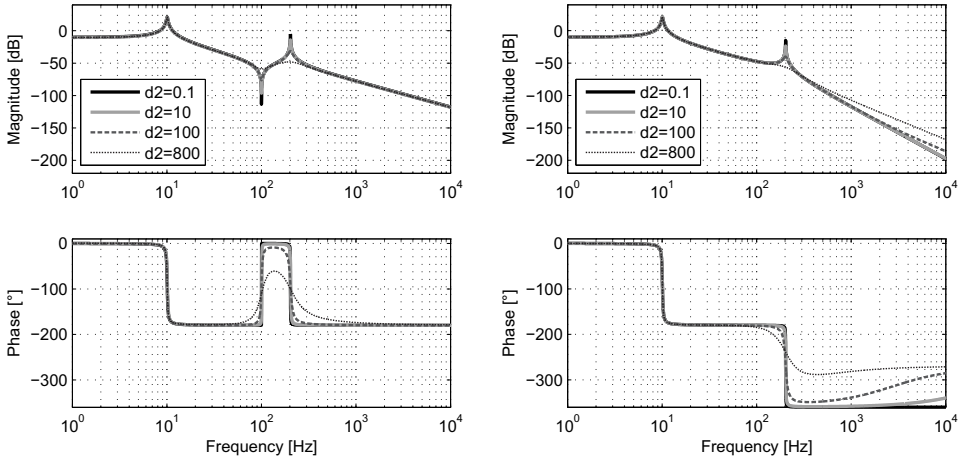

(a) First body TF. (b) Second body TF.

Fig. 2. Simulated influence of the damping coefficient d_2 (in N·s/m) on the decoupling behavior. (a) shows the TF of the first body with a resonance of the suspension mode at f_1=10 Hz, an anti-resonance at f_a=100 Hz and a decoupling resonance at f_2=203 Hz. The mass line after the decoupling is vertically shifted. An increased d_2 reduces the peak heights at the anti-resonance and the decoupling resonance. (b) shows the TF of the second body with a suspension mode and a decoupling resonance at f_1 and f_2, respectively. An increased d_2 reduces the decoupling effect.

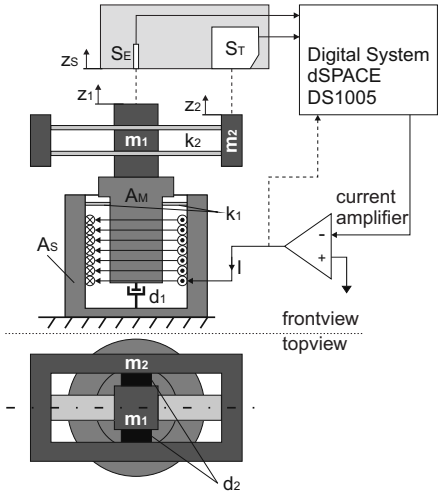

Fig. 3. Schematic of the experimental setup. S_E and S_T are sensors for measuring positions z_1 and z_2, respectively. m_1 and m_2 represent the inner and outer body, k_2 the spring constant of the connecting leaf springs and d_2 the damping between inner and outer body. d_1 and k_1 are the damping and spring constant inside the actuator. The amplifier drives the actuator with stator A_S and mover A_M. z_s is the position of the sensor system, affected by external vibrations.

long, 40 mm wide) forming the spring k_2. Two leaf springs are used to provide guidance in vertical direction while minimizing torsional movement of the outer body. To introduce additional damping d_2 the profiles of the outer body parallel to the leaf springs are clamped to the inner body with a single sheet of damping material (Sorbothane) in-between on both sides (see black blocks in Fig.3).

For measuring the position of the inner body z_1 an eddy current sensor S_E (eddyNCDT DT3702-U1-A-C3, Micro-Epsilon GmbH, Germany) with a resolution of 1.3 nm is used. Monitoring the position of the outer body z_2 is performed by an optical triangulation sensor S_T (optoNCDT 2300, Micro-Epsilon GmbH, Germany). External disturbances like floor vibrations are considered to affect the position of both, the inner and the outer body. The input of the system is the input of the current amplifier u, which via the motor constant exerts a force on the moving masses. The TF from u to the position of the inner body z_1 and the outer body z_2 is defined by G_{iB} and G_{oB} (see (3) and (4)), respectively. The distance between sensor and inner body $y_1 = z_1 - z_s$ is considered as the controlled system output.

IV. System Identification

To identify the dynamic behavior of the experimental setup the current of the power amplifier is driven by a sinusoidal signal which is logarithmically increasing in frequency. For measuring the TF of the inner and outer body, the position of the respective body, y_1 or y_2, is the corresponding system output. The magnitude and phase response are determined by the lock-in principle using the dSPACE-platform running at 20 kHz [26]. Fig.4 depicts the measured frequency response of the inner and the outer body and the manually fitted system models. The resonance/anti-resonance frequencies are derived by identifying the local maxima/minima in the magnitude plot data.

The measured frequency response of the inner body in Fig.4(a) has the same shape as the model derived in Section II

Post-print version of the article: E. Csencsics and M. Thier and R. Hainisch and G. Schitter, "System and control design of a voice coil actuated mechanically decoupling two-body vibration isolation system," *IEEE Transactions on Mechatronics*, vol. 23, no. 1, pp. 321-330, 2018. DOI: 10.1109/TMECH.2017.2771440

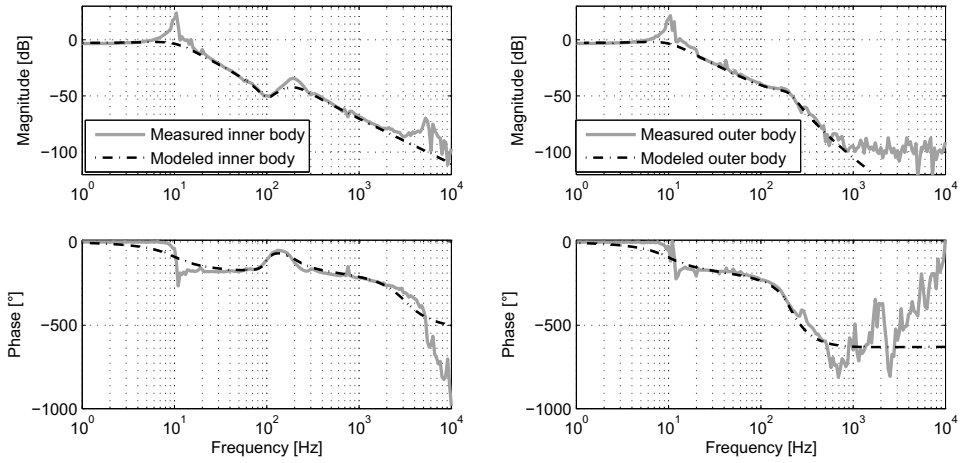

(a) (b)

Fig. 4. Measured and modeled frequency response of the inner and the outer body. (a) shows the TF of the inner body, with a suspension mode at 10 Hz. The anti-resonance is located at 100 Hz and the decoupling resonance at 190 Hz. (b) shows the TF of the outer body with the same resonance frequencies as the inner body. A -60 dB slope can be obtained above the zero at 338 Hz. The time delay of the optical sensor prevents an observation of the recovering phase.

up to a frequency of about 3 kHz. At higher frequencies additional structural modes can be observed. The first resonance peak due to the actuator suspension and the entire moved mass appears at 10 Hz. The anti-resonance and resonance of the decoupling are located at around 100 Hz and 190 Hz, respectively, and are both well damped (modeled d_2=800 N·s/m). Structural modes of the outer body (e.g. around 400 Hz), lying above the target bandwidth of *MS2* (equals the decoupling resonance) and below the target bandwidth of *MS1*, which would affect the dynamics of a rigid design, would practically not be observable in the TF of the inner body of the decoupling design, as their excitation is reduced by the decoupling. According to the measured data and the mass ratio the mass line is lifted about 12 dB after the decoupling resonance. Based on the measured data the fitted system model for the inner body

$$G_{iB}(s) = K \cdot G_{z1,F} \cdot Pa_i(s), \tag{13}$$

with $G_{z1,F}$ from (3) and parameters according to Table II is obtained. $Pa_i(s)$ is a second order Pade-approximation [27] that accounts for the sampling delay of T_s=50 μs of the digital system. The dynamics of the current amplifier are neglected. Considering the targeted control design, which at low frequencies is influenced by the suspension mode occurring at 10 Hz, the model is deliberately shaped in this frequency range.

Fig.4(b) shows the frequency response of the outer body, with a shape corresponding to the theoretical model in Fig. 2(b). It shows the suspension mode, as the inner body, at 10 Hz followed by a -40 dB mass line. At about 190 Hz the outer body decouples, which is indicated by the second strongly damped resonance and a related phase drop, such that above this frequency a forth order behavior with a -80 dB slope can be obtained. The zero due to the damping at f_z =338 Hz (see (10)) reduces the slope to -60 dB. The noise floor for the outer body is located around -100dB. Based on the measured data the fitted system model for the outer body

$$G_{oB}(s) = K \cdot G_{z2,F} \cdot Pa_o(s), \tag{14}$$

with $G_{z2,F}$ from (4) and parameters according to Table II is obtained. $Pa_o(s)$ is a second order Pade-approximation [27] that is used to model the phase lag due to the delay of the optical sensor of about 2 ms below 500 Hz. This time delay prevents an observation of the recovering phase as would be expected from the theoretical model (see Fig. 2), since the noise floor of the sensor is reached.

TABLE II
COEFFICIENTS OF THE FITTED SYSTEM MODELS FOR THE TFS DESCRIBED IN (13) AND (14).

Parameter	Value	Unit
m_1	1.4	kg
m_2	4.3	kg
k_1	23e3	N/m
k_2	17e5	N/m
d_1	400	N·s/m
d_2	800	N·s/m
K	1.686e4	-

V. CONTROLLER DESIGN FOR SINGLE AXIS DECOUPLING SYSTEM

From a controls perspective aiming to position the first body with a bandwidth above the decoupling frequency two system design aspects are favorable:

Post-print version of the article: E. Csencsics and M. Thier and R. Hainisch and G. Schitter, "System and control design of a voice coil actuated mechanically decoupling two-body vibration isolation system," *IEEE Transactions on Mechatronics*, vol. 23, no. 1, pp. 321-330, 2018. DOI: 10.1109/TMECH.2017.2771440

(i) High damping coefficient ζ_a for anti-resonance at f_a: A low ζ_a would be compensated by a high resonance in the controller which is not recommendable in the face of the mechanical system properties, robustness against plant variations and controller saturation.
(ii) High damping coefficient ζ_2 for resonance at f_2 (decoupling frequency): To avoid extensive excitation of the second body at this frequency, due to external disturbances.

The damping d_2 between first and second body is thus an important design parameter for increasing the controllability of the proposed system, as it can be used to increase these damping coefficients (see Fig. 2). This leads to a tradeoff in the system design as d_2 needs to be chosen such that the peaking is sufficiently reduced, while the decoupling of the second body is not too much compromised.

A. Controller Design

To design a controller for G_{iB} (see (13)) an H_∞ approach is used [27]. Starting from a *Mixed Sensitivity Problem* [28] the extended model shown in Fig. 5a is employed for controller synthesis. To ensure robustness of the controller against

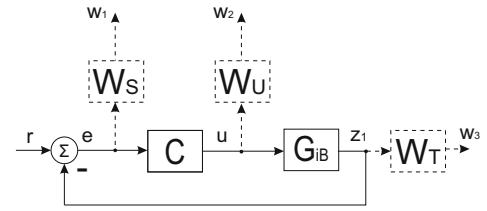

(a) Extended model.

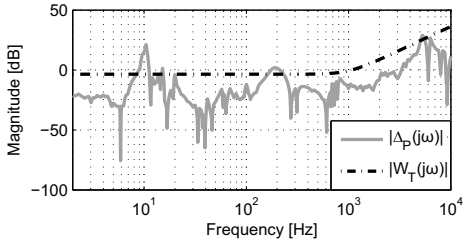

(b) Multiplicative model uncertainty.

Fig. 5. H_∞ controller synthesis. (a) shows the extended model with $C(s)$ being the controller, $G_{iB}(s)$ the plant and W_S, W_U, and W_T being the weighting functions. (b) depicts the multiplicative model uncertainty (solid, grey) according to the model error of the inner body model and its upper border W_T.

unmodeled system dynamics the error between the measured plant data $\tilde{P}(s)$ and the fitted plant model $P(s)$ is introduced in the form of a multiplicative system uncertainty:

$$\Delta_P(s) = \frac{\tilde{P}(s) - P(s)}{P(s)}. \tag{15}$$

For considering this uncertainty in the controller design, $\Delta_P(s)$ is approximated by the function

$$W_T(s) = 0.67e8 \cdot \frac{s^2 + 2\zeta\omega_N s + \omega_N^2}{s^2 + 2\zeta\omega_D s + \omega_D^2}, \tag{16}$$

as shown in Fig. 5b with ω_N= 6.28e3 rad/s, ω_D= 6.28e7 rad/s, and ζ=0.7, acting as an upper limit of the uncertainty. The larger error at 10 Hz is neglected, as it is due to the overdamped suspension mode in the system model (see Fig. 4) and significantly lower than the targeted cross over frequency. The modeled suspension mode is deliberately higher damped to avoid cancellation of this resonance in the controller design. This anti-resonance would compromise the rejection of external vibrations at this frequency, so that it is beneficial to employ the high gain at the resonance to improve robustness against external disturbances. In the sense of the *Small Gain Theorem* the function W_T is used as a lower border for all potential weighting functions for $T(s) = C(s)P(s)/[1 + C(s)P(s)]$ [29]. For shaping the disturbance rejection a first order function with inverted highpass characteristic is chosen for the weighting function of $S(s) = 1/[1 + C(s)P(s)]$:

$$W_S(s) = 0.2 \cdot \frac{s + 6.28e3}{s + 0.628}. \tag{17}$$

To enforce a reduced control effort at higher frequencies the requirement on $U(s) = P(s)/[1 + C(s)P(s)]$ is formulated by a first order function with inverted lowpass characteristic:

$$W_U(s) = 0.7071 \cdot \frac{s + 1.26e3}{s + 1.26e7}. \tag{18}$$

Given the system model defined in (13) and the weighting functions, the resulting controller is of 7th order:

$$C(s) = K_H \cdot \frac{\prod_{i=1}^{2} s^2 + 2\zeta_{z_i}\omega_{z_i} s + \omega_{z_i}^2}{\prod_{i=1}^{2} s^2 + 2\zeta_{p_i}\omega_{p_i} s + \omega_{p_i}^2 \cdot \prod_{i=3}^{5} s + \omega_{p_i}}, \tag{19}$$

with K_H=6.5912e16 and coefficients according to Table III.

TABLE III
COEFFICIENTS OF THE DESIGNED CONTROLLER C.

Index	ω_{Index} [rad/s]	ζ_{Index}
z_1	63.6	0.55
z_2	1270	0.38
p_1	631	0.15
p_2	18200	0.36
p_3	0.5	-
p_4	20500	-
p_5	41200	-

B. Controller Implementation

For implementation in the processor of the dSPACE system the controller is discretized using *Pole-Zero-Matching* [30], such that poles and zeros of the digital and continuous controller are matching over the entire frequency range. Fig.6 depicts the measured TF of the obtained controller.

At frequencies below 200 Hz the shape of the controller almost equals the inverse plant dynamics with an additional I-gain below 10 Hz, due $W_S(s)$. It can be seen that due to the modeling there is no notch in the controller at 10 Hz to cancel the suspension mode. Due to the damping between inner an outer body there is a highly damped pair of zeros

Post-print version of the article: E. Csencsics and M. Thier and R. Hainisch and G. Schitter, "System and control design of a voice coil actuated mechanically decoupling two-body vibration isolation system," *IEEE Transactions on Mechatronics*, vol. 23, no. 1, pp. 321-330, 2018. DOI: 10.1109/TMECH.2017.2771440

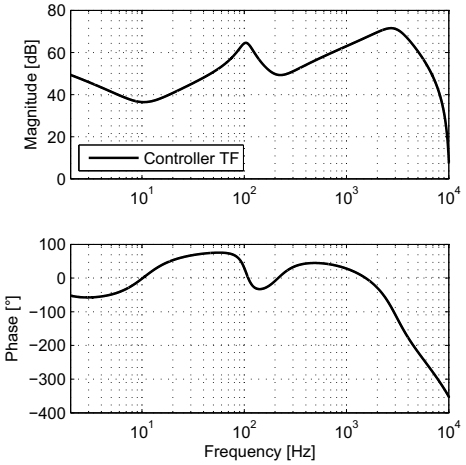

Fig. 6. Measured controller frequency response of the designed controller to control the position of the inner body. With the applied system model there results no notch filter at the suspension mode (10 Hz). There is a highly damped pair of zeros at the decoupling frequency 190 Hz and also a highly damped pair of poles at 100 Hz to compensate the anti-resonance.

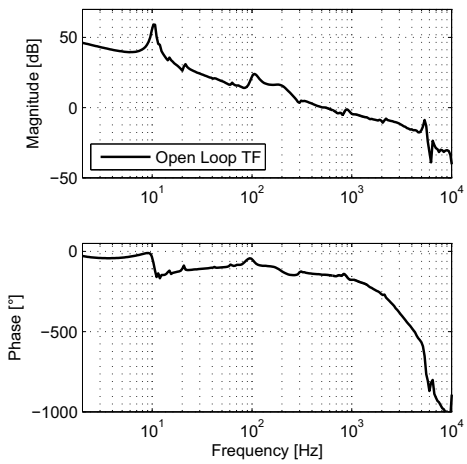

Fig. 7. Measured open loop frequency response of the system with the designed controller for controlling the position of the inner body. It shows a cross over frequency of 550 Hz with a phase margin of 45°.

at the decoupling frequency of 190 Hz and more important a highly damped pair of poles at 100 Hz to compensate for the anti-resonance. Due to $W_U(s)$ the controller gain decreases rapidly above 3 kHz.

VI. Validation and Results

The measured open loop TF with the implemented controller is depicted in Fig. 7. It shows a cross over frequency of 550 Hz with a phase margin of 45° and a gain margin of 5 dB. The additional structural mode of the plant at around 5.5kHz (see Fig. 4(a)) was not modeled during system identification and does not impair the closed loop system stability.

The measured complementary sensitivity function for reference tracking of the inner and the outer body is shown in Fig. 8. Additionally the TFs computed from the system models and the designed controller are depicted (dash dotted lines). Both measurements are in good agreement with the modeled response. The inner body shows a -3 dB bandwidth of 1.4 kHz and follows a -40 dB slope right above it. The deviations between model and measurement around 5 kHz result from the unmodeled structural mode of the plant (see Fig. 4(a)). The measured complementary sensitivity function of the outer body shows a -3 dB bandwidth of around 180 Hz, which is in the range of the designed decoupling frequency. It results from a multiplication of the complementary sensitivity function of the inner body with $G_{z2,z1}$ (see (8)). This clearly explains its shape, the resulting bandwidth, the gain peak of about 12 dB below, and the -40 dB slope right above the bandwidth until the zero due to the damping at f_z =338 Hz. This zero reduces the slope to a -20dB slope until the poles from the complementary sensitivity function of the inner body increase it again. A reduction of the gain peak would thus only be possible by introduction of higher damping. The large phase deviations above 100 Hz result from the unmodeled delay of the optical position sensor of about 2 ms.

This shows that the bandwidths of the two subsystems can be designed independently from each other for a given application, as long as they are well separated and the bandwidth of the inner body is the larger one. The bandwidth of the inner body is determined by the controller design itself, while the bandwidth of the outer body is determined by the designed decoupling frequency.

To demonstrate the importance of the damping parameter d_2 for the system performance, Fig. 9 compares 10 μm step responses of the experimental system (d_2=800) and a weakly damped decoupling system (d_2=10). Fig. 9a shows the step response of the inner bodies of both systems, controlled with related feedback controllers ($C(s)$ for the experimental system). The controller design (see Section V) for the weakly damped system yields a controller with a sharp inverse notch at the anti-resonance. It can be seen that both responses are comparable, with the weakly damped system, however, showing long but small transient oscillations with the frequency of the anti-resonance. They result from slight mismatches between plant anti-resonance and controller resonance, which will always be present in a practical system. Looking at the step response of the outer body in Fig. 9b, reveals that there are significantly higher and longer transients in the weakly damped system, preventing a fast repositioning of the outer body. These large transients are due to the high peak in the complimentary sensitivity function of the outer body, caused by the weakly damped anti-resonance (compare Fig. 8), which also impairs the disturbance rejection performance of the outer body (compare Fig. 11). A simulation study also shows that assuming a slightly deviating anti-resonance (<3%), which can easily happen due to e.g. thermal or mechanical drift, the

Post-print version of the article: E. Csencsics and M. Thier and R. Hainisch and G. Schitter, "System and control design of a voice coil actuated mechanically decoupling two-body vibration isolation system," *IEEE Transactions on Mechatronics*, vol. 23, no. 1, pp. 321-330, 2018. DOI: 10.1109/TMECH.2017.2771440

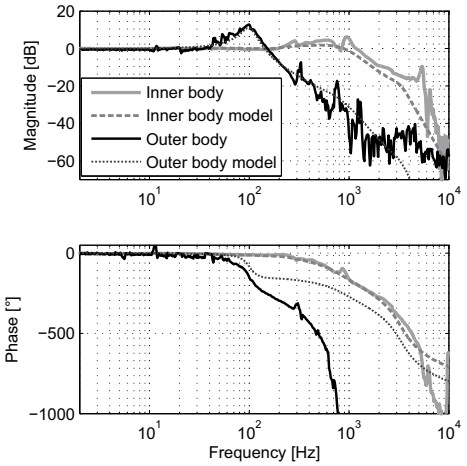

Fig. 8. Measured and modeled complementary sensitivity functions. The position of the inner body is controlled. The inner body has a -3 dB bandwidth of 1.4 kHz while the outer body has a -3dB bandwidth around the decoupling frequency at 180 Hz. The measured TFs show good matching with the modeled system response.

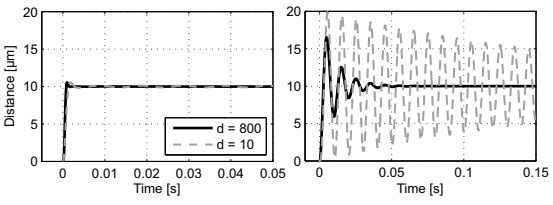

Fig. 9. Simulated 10 μm step responses of experimental and weakly damped system with related feedback controllers. (a) shows the responses of the actively controlled inner bodies. (b) shows the responses of the outer bodies with significantly longer transients in the weakly damped system.

weakly damped system already becomes unstable. This clearly validates the importance of d_2 in the system design.

The measured response of the inner and outer body of the experimental system to a step of 10 μm height is depicted in Fig. 10. It corresponds to the case of repositioning the two bodies of the system, as in the case of changing the operating point of the combined metrology system introduced in Section I. From the zoomed image in Fig. 10(b) it can be seen that the response of the inner body has a rise time of about 1.2 ms and an overshoot of 12.4%. The response of the outer body shows a time delay according to the delay of the used optical sensor. It has a rise time of about 3.3 ms and an overshoot of 34.1%. The inner body, the high precision part, thus shows good tracking (repositioning) performance with none of the significant oscillations of the outer body observable. The outer body, the low precision part, also shows good but slower tracking of the reference with increased overshoot and oscillations. The remaining positioning error

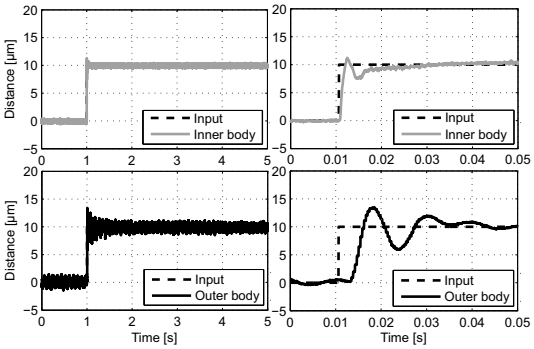

(a) Step response (b) Zoomed step response

Fig. 10. Measured step responses of the inner (grey) and the outer body (black) for an input step of 10 μm. (a) shows the step responses and (b) the zoomed areas around the step. The inner body follows the step with a rise time of 1.2 ms and shows small overshoot. The rise time of the outer body is 3 times longer, the overshoot is with 34% higher, and the settling time is longer.

(for a laboratory environment with vibrations of 2.24 μm rms) shows a standard deviation of 113 nm for the inner body and 514 nm for the outer, not actively controlled, body. From these results it can be seen that the slower and less precise motion of the outer body does not impair the performance of the inner body, which is clear, as the interaction between the two bodies is already included in the dynamic model and is thus handled by the position controller.

The measured sensitivity function of the controlled inner body is shown in Fig. 11 together with its inverse weighting function W_S. It crosses the 0 dB line at 380 Hz and attains a peak of about 10 dB, due to the *Waterbed effect* [1], right after at about 700 Hz. Due to the controller design the suspension mode of the system is not canceled, such that its high gain results in an improved disturbance rejection around 10 Hz. The disturbance rejection performance of the outer body can not be measured but only estimated using the derived system models (see (3)-(8)) with the fitted parameters and the controller TF. With external disturbances affecting both bodies it results in

$$S_{outer}(s) = G_{z2,z1}\frac{C \cdot G_{iB}}{1 + C \cdot G_{iB}} - 1. \qquad (20)$$

Above 10 Hz it shows a decreased disturbance rejection as compared to one of the inner body, crossing the 0 dB line at 70 Hz and attaining a peak around 100 Hz.

To evaluate the disturbance rejection performance in the time domain a displacement disturbance profile is derived. The disturbance profile is calculated using the spectral BBN VC-A criterion [31], assuming a constant velocity magnitude above the defined frequency range of the criterion (4-80 Hz) to calculate the displacement disturbance signal. The displacement disturbance signal is used as reference, while the error between reference and current position is considered as output. This relation results in an equal TF as the disturbance (z_s) to output (y_1) relation. The resulting positioning error of inner and outer body is depicted in Fig. 12. The positioning error of

Post-print version of the article: E. Csencsics and M. Thier and R. Hainisch and G. Schitter, "System and control design of a voice coil actuated mechanically decoupling two-body vibration isolation system," *IEEE Transactions on Mechatronics*, vol. 23, no. 1, pp. 321-330, 2018. DOI: 10.1109/TMECH.2017.2771440

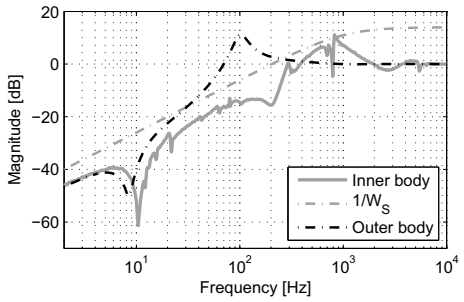

Fig. 11. Measured sensitivity function of the closed loop system. The sensitivity function of the inner body (solid, grey) crosses the 0 dB line at 380 Hz and has a peak value of 10 dB. The inverse of the weighting function W_S (dash-dotted, grey) represents an upper bound. The model-based estimation of the disturbance rejection of the outer body (dash-dotted, black) from (20) shows a reduced performance above 5 Hz.

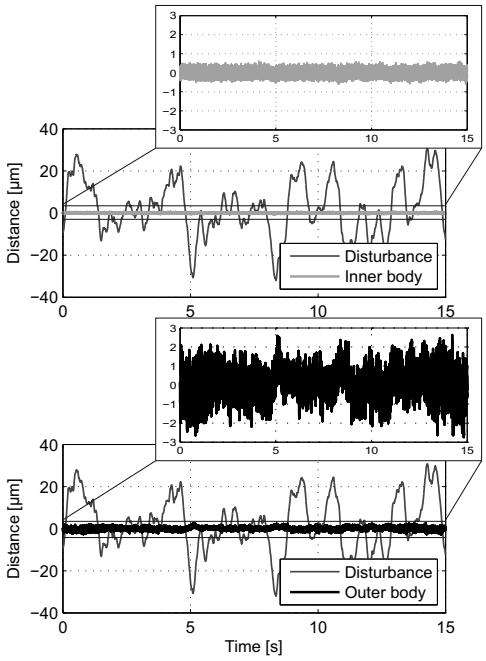

Fig. 12. Disturbance rejection of the inner (top, grey) and outer (bottom, black) body of the closed loop system. The disturbance (dark grey) with 62.8 μm peak-peak and 12.4 μm rms value is applied. The controlled inner body shows a peak-peak error of 1.21 μm and a rms value of 0.12 μm. The not actively controlled outer body shows a peak-peak position error value of 5.37 μm and a rms value of 0.81 μm.

the inner body shows a peak-peak value of 1.21 μm and a rms value of 0.12 μm. Even though the outer body is not actively controlled, it also provides significant disturbance rejection. The resulting positioning errors of 5.37 μm peak-peak and 0.81 μm rms correspond to a reduction of the disturbance profile of 91.4% and 93.5%, respectively.

In summary the proposed system design enables vibration isolation with a bandwidth of 1.4 kHz for the inner body and 180 Hz for the outer body, respectively, by the designed H_∞-controller. Thereby the system enables a significant reduction of vibrational disturbances for both bodies of the vibration isolation system.

VII. Conclusion

In this paper a decoupling mechanism is proposed as a design choice for a combined metrology system with a high and low precision subsystem and a controller design to actively control the position of the high precision subsystem is introduced. The system analysis and design reveal and explain that the damping in the system as an important design parameter for the robustness of the feedback system and the performance of the outer subsystem. An experimental setup of a single DoF decoupling system with a decoupling frequency of about 190 Hz is developed, showing good agreement with the analytical description. The designed model-based H_∞-controller actively controls the position of the inner body, and is designed based on a system model with a deliberately overdamped suspension mode, resulting in an improved disturbance rejection of the closed loop system. It is shown that with this controller the inner and the outer body of the built prototype can simultaneously be controlled with bandwidths of 1.4 kHz and 180 Hz, respectively. Exposed to a disturbance profile according to the BBN VC-A criterion with 12.4 μm rms value in the laboratory environment, it is shown that the remaining rms positioning errors for the actively and passively controlled body can be reduced to 0.12 μm and 0.81 μm, respectively. For matters of integration, ease of tuning and the further experimental investigation of the effects of various damping values, nicely tunable compact damping mechanisms are required in the future.

Acknowledgment

The authors acknowledges funding from the EU commission under the FP7 NMP Programme, project title aim4np, grant number 309558.

References

[1] R. Munnig Schmidt, G. Schitter, A. Rankers, and J. van Eijk, *The Design of High Performance Mechatronics*, 2nd ed. Delft University Press, 2014.
[2] H. Amick, M. Gendreau, T. Busch, and C. Gordon, "Evolving criteria for research facilities: vibration," *Optics & Photonics 2005*, p. 593303, 2005.
[3] A. Carrella, M. Brennan, and T. Waters, "Static analysis of a passive vibration isolator with quasi-zero-stiffness characteristic," *Journal of Sound and Vibration*, vol. 301, no. 3, pp. 678–689, 2007.
[4] E. I. Rivin, *Passive vibration isolation*. New York: ASME press, 2003.
[5] Y. Kim, S. Kim, and K. Park, "Magnetic force driven six degree-of-freedom active vibration isolation system using a phase compensated velocity sensor," *Review of Scientific Instruments*, vol. 80, no. 4, 2009.
[6] L. Zuo and J. J. E. Slotine, "Robust vibration isolation via frequency-shaped sliding control and modal decomposition," *Journal of Sound and Vibration*, vol. 285, no. 4, pp. 1123–1149, 2005.
[7] M. Thier, R. Saathof, E. Csencsics, R. Hainisch, A. Sinn, and G. Schitter, "Design and control of a positioning system for robot-based nanometrology," *at-Automatisierungstechnik*, vol. 63, no. 9, pp. 727–738, 2015.
[8] S. Ito, D. Neyer, S. Pirker, J. Steininger, and G. Schitter, "Atomic force microscopy using voice coil actuators for vibration isolation," *2015 IEEE International Conference on Advanced Intelligent Mechatronics (AIM)*, pp. 470–475, 2015.

[9] S. Ito, J. Steininger, and G. Schitter, "Low-stiffness dual stage actuator for long rage positioning with nanometer resolution," *Mechatronics*, vol. 29, pp. 46–56, 2015.
[10] G. Schitter, K. J. Astrom, B. E. DeMartini, P. J. Thurner, K. L. Turner, and P. K. Hansma, "Design and modeling of a high-speed afm-scanner," *IEEE Transactions on Control Systems Technology*, vol. 15, no. 5, pp. 906–915, 2007.
[11] B. Babakhani and T. J. De Vries, "Active damping of the 1d rocking mode," *International Conference on Mechatronics and Automation (ICMA), IEEE*, pp. 1370–1375, 2010.
[12] M. G. E. Schneiders, M. J. G. van de Molengraft, and M. Steinbuch, "Introduction to an integrated design for motion systems using overactuation," *Proceedings of the European Control Conference*, 2003.
[13] E. T. Falangas, J. A. Dworak, and S. Koshigoe, "Controlling plate vibrations using piezoelectric actuators," *Control System IEEE*, vol. 14, no. 4, pp. 34–41, 1994.
[14] X. Wei and J. E. Mottershead, "A block decoupling control algorithm for vibration suppression of linear structures," *Mechanism and Machine Science*, vol. 23, pp. 329–338, 2014.
[15] T. Nestorovic and M. Trajkov, "Optimal actuator and sensor placement based on balanced reduced models," *Mechanical Systems and Signal Processing*, vol. 36, no. 2, pp. 271–289, 2013.
[16] T. Bartel, H. Atzrodt, S. Herold, and T. Melz, "Modelling of an active mounted plate by means of the superposition of a rigid body and an elastic model," *Proceedings of ISMA2010*, pp. 511–523, 2010.
[17] J. Giaime, P. Saha, D. Shoemaker, and L. Sievers, "A passive vibration isolation stack for ligo: design, modeling, and testing," *Review of scientific instruments*, vol. 67, no. 1, pp. 208–214, 1996.
[18] S. Pirro, "Further developments in mechanical decoupling of large thermal detectors," *Nuclear Instruments and Methods in Physics Research Section A: Accelerators, Spectrometers, Detectors and Associated Equipment*, vol. 559, no. 2, pp. 672–674, 2006.
[19] C. Acar and A. M. Shkel, "Nonresonant micromachined gyroscopes with structural mode-decoupling," *Sensors Journal, IEEE*, vol. 3, no. 4, pp. 497–506, 2003.
[20] Z. Lu, M. J. Brennan, and L.-Q. Chen, "On the transmissibilities of nonlinear vibration isolation system," *Journal of Sound and Vibration*, vol. 375, pp. 28–37, 2016.
[21] A. Shaw, S. Neild, D. Wagg, P. Weaver, and A. Carrella, "A nonlinear spring mechanism incorporating a bistable composite plate for vibration isolation," *Journal of Sound and Vibration*, vol. 332, no. 24, pp. 6265–6275, 2013.
[22] X. Huang, X. Liu, J. Sun, Z. Zhang, and H. Hua, "Vibration isolation characteristics of a nonlinear isolator using euler buckled beam as negative stiffness corrector: A theoretical and experimental study," *Journal of Sound and Vibration*, vol. 333, no. 4, pp. 1132–1148, 2014.
[23] X. Sun, X. Jing, J. Xu, and L. Cheng, "Vibration isolation via a scissor-like structured platform," *Journal of Sound and Vibration*, vol. 333, no. 9, pp. 2404–2420, 2014.
[24] E. Coelingh, T. J. De Vries, and R. Koster, "Assessment of mechatronic system performance at an early design stage," *IEEE/ASME Transactions on Mechatronics*, vol. 7, no. 3, pp. 269–279, 2002.
[25] A. M. Rankers, *Machine Dynamics in Mechatronic Systems: An Engineering Approach*. Philips Electronics N.V., 1997.
[26] J. M. Masciotti, J. M. Lasker, and A. H. Hielscher, "Digital lock-in detection for discriminating multiple modulation frequencies with high accuracy and computational efficiency," *IEEE Transactions on Instrumentation and Measurement*, vol. 57, no. 1, pp. 182–189, Jan 2008.
[27] S. Skogestad and I. Postlethwaite, *Multivariable Feedback Control*. John Wiley, New York, 2005.
[28] H. Kwakernaak, "Robust control and h_∞-optimization - tutorial paper," *Automatica*, vol. 29, no. 2, pp. 255–273, 1993.
[29] T. Yamaguchi, M. Hirata, and C. Pang, *High-Speed Precision Motion Control*. Taylor & Francis, 2011.
[30] G. Franklin, D. Powell, and M. Workman, *Digital Control of Dynamic Systems*. Prentice Hall, 1997.
[31] C. G. Gordon, "Generic vibration criteria for vibration-sensitive equipment," *SPIE's International Symposium on Optical Science, Engineering, and Instrumentation. International Society for Optics and Photonics*, pp. 22–33, 1999.

Ernst Csencsics Ernst Csencsics is PhD student at the Automation and Control Institute (ACIN) at Vienna University of Technology. He received a MSc. degree in Electrical Engineering from TU Vienna, Austria (2014).

His primary research interests are on high performance mechatronic systems design, control of opto-mechatronic systems, precision engineering, and in-line metrology systems.

Markus Thier Markus Thier is PhD student at the Automation and Control Institute (ACIN) at Vienna University of Technology. He received a MSc. degree in Electrical Engineering from TU Vienna, Austria (2012).

His primary research interests are on mechatronic systems design, precision engineering and vibration isolation for in-line metrology, real time systems for signal processing, and wave front sensing.

Reinhard Hainisch Reinhard Hainisch is researcher at the Automation and Control Institute (ACIN) at Vienna University of Technology since 2013. He received a MSc. in Electrical and Biomedical Engineering from Graz University of Technology, Austria (2003) and his PhD degree from Vienna University of Technology, Austria (2015).

His primary research interests are in the field of system design and medical engineering.

Georg Schitter Georg Schitter is Professor at the Automation and Control Institute (ACIN) of the Vienna University of Technology. He received a MSc. in Electrical Engineering from TU Graz, Austria (2000) and his PhD degree from ETH Zurich, Switzerland (2004).

His primary research interests are on high-performance mechatronic systems and multidisciplinary systems integration, particularly for precision engineering applications in the high-tech industry, scientific instrumentation, and mechatronic imaging systems, such as scanning probe microscopy, adaptive optics, and lithography systems for semiconductor industry.

He serves as Associate Editor for the IEEE/ASME Transactions on Mechatronics (2010-2014) as well as for the IFAC Journals Control Engineering Practice and IFAC Mechatronics.

Post-print version of the article: E. Csencsics and M. Thier and R. Hainisch and G. Schitter, "System and control design of a voice coil actuated mechanically decoupling two-body vibration isolation system," *IEEE Transactions on Mechatronics*, vol. 23, no. 1, pp. 321-330, 2018. DOI: 10.1109/TMECH.2017.2771440